AJNR

In Vivo ^{1}H MR Spectroscopy of Human Head and Neck Lymph Node Metastasis and Comparison with Oxygen Tension Measurements

Josh M. Star-Lack, Eifar Adalsteinsson, Markus F. Adam, David J. Terris, Harlan A. Pinto, J. Martin Brown and Daniel M. Spielman

AJNR Am J Neuroradiol 2000, 21 (1) 183-193
http://www.ajnr.org/content/21/1/183

AJNR Am J Neuroradiol 21:183–193, January 2000

In Vivo ^{1}H MR Spectroscopy of Human Head and Neck Lymph Node Metastasis and Comparison with Oxygen Tension Measurements

Josh M. Star-Lack, Eifar Adalsteinsson, Markus F. Adam, David J. Terris, Harlan A. Pinto, J. Martin Brown, and Daniel M. Spielman

BACKGROUND AND PURPOSE: **Current diagnostic methods for head and neck metastasis are limited for monitoring recurrence and assessing oxygenation. ^{1}H MR spectroscopy (^{1}H MRS) provides a noninvasive means of determining the chemical composition of tissue and thus has a unique potential as a method for localizing and characterizing cancer. The purposes of this investigation were to measure ^{1}H spectral intensities of total choline (Cho), creatine (Cr), and lactate (Lac) in vivo in human lymph node metastases of head and neck cancer for comparison with normal muscle tissue and to examine relationships between metabolite signal intensities and tissue oxygenation status.**

METHODS: **Volume-localized Lac-edited MRS at 1.5 T was performed in vivo on the lymph node metastases of 14 patients whose conditions were untreated and who had primary occurrences of squamous cell carcinoma. MRS measurements were acquired also from the neck muscle tissue of six healthy volunteers and a subset of the patients. Peak areas of Cho, Cr, and Lac were calculated. Tissue oxygenation (pO_2) within the abnormal lymph nodes was measured independently using an Eppendorf polarographic oxygen electrode.**

RESULTS: **Cho:Cr ratios were significantly higher in the nodes than in muscle tissue (node Cho:Cr = 2.9 ± 1.6, muscle Cho:Cr = 0.55 ± 0.21, $P = .0006$). Lac was significantly higher in cancer tissue than in muscle ($P = .01$) and, in the nodes, showed a moderately negative correlation with median pO_2 ($r = -.76$) over a range of approximately 0 to 30 mm Hg. Nodes with oxygenation values less than 10 mm Hg had approximately twice the Lac signal intensity as did nodes with oxygenation values greater than 10 mm Hg ($P = .01$). Cho signal intensity was not well correlated with pO_2 ($r = -.46$) but seemed to decrease at higher oxygenation levels (>20 mm Hg).**

CONCLUSION: **^{1}H MRS may be useful for differentiating metastatic head and neck cancer from normal muscular tissue and may allow for the possibility of assessing oxygenation. Potential clinical applications include the staging and monitoring of treatment.**

In vivo ^{1}H MR spectroscopy (^{1}H MRS) has been shown to offer a noninvasive means of detecting the presence of active tumor. Typical spectral patterns associated with cancer include an increase in the total choline (Cho, 3.2 ppm) signal intensity (SI) relative to creatine (Cr, 3.0 ppm), often coupled with the presence of other metabolites, including lactate (Lac, 1.3 ppm) (1–5). Both diagnostic and oncologic applications may be offered by allowing for discrimination between regions of healthy tissue, necrosis, and new growth or recurrence (6, 7). Although, in the past, the majority of studies have been conducted in the human brain, there is growing interest in proton MRS of other organs if technical difficulties can be overcome (8).

^{1}H MRS has recently been proposed as a means to localize head and neck cancer and monitor therapy. In vitro and in vivo studies by Mukherji et al (9, 10) confirmed that increased Cho:Cr ratios were evident in pretreated squamous cell carcinoma. In vivo data were acquired mainly from the tongue base, which was the primary site of occurrence, thus suggesting future studies of in vivo spectral

Received October 26, 1998; accepted after revision July 22, 1999.

From the Lucas MRS Imaging Center (J.S.L., E.A., D.M.S.), Department of Radiology, the Department of Radiation Oncology/Division of Radiation Biology (M.F.A., J.M.B.), the Division of Otolaryngology/Head and Neck Surgery (D.J.T.), and the Department of Veterans Affairs Palo Alto Health Care System and Oncology Division Department of Medicine (H.A.P.), Stanford University, Stanford, CA.

Address reprint requests to Daniel Spielman, Lucas MRS Imaging Center, Department of Radiology, Stanford University, MC 5488, Stanford, CA 94305.

characteristics of metastatic nodes. A case study by van Zijl et al (11) showed that effective radiation treatment caused a complete disappearance of metabolite signals in a neck node metastasis. Lac has been detected in vivo in pretreated human head and neck tumors in two feasibility studies (12, 13).

In addition to verifying the presence of active tumor, ^{1}H MRS may offer the possibility of helping to monitor the oxygenation status of the neoplasm. This could be particularly relevant to treatment planning because tumor hypoxia has been shown to be associated with increased resistance to radiation therapy and chemotherapy (14−17). The current standard of reference for measuring tumor oxygenation (pO_2) is the computerized Eppendorf oxygen electrode (18−20), which, unfortunately, is invasive and may not be suitable as a screening device.

One potential means of assessing tumor oxygenation with proton MRS is to measure Lac SI as a marker for nonoxidative glycolysis. Lac is a redox partner of pyruvate, which is a metabolic intermediate between glycolysis and the Krebs or tricarboxylic acid cycle. When oxygen availability is low because of a perfusion deficit or other metabolic stress, the tricarboxylic acid cycle rate drops and pyruvate produced during glycolysis may be converted to Lac. In MRS studies of the human brain, Lac has been detected in areas of low perfusion resulting from such insults as ischemic stroke (21, 22) and neonatal asphyxia (23).

It is not known to what extent Lac signal intensities are reflective of oxygenation in tumors, which are inherently less aerobic than normal parenchyma. Lac levels can be a function of several factors, including perfusion, metabolic rates, glucose supply, and the concentration of certain enzymes such as Lac dehydrogenase (24−27). In vivo MRS studies of human brain cancer offer contradictory evidence regarding whether total Lac SI is correlated with total metabolic activity (as measured via ^{18}F-fluorodeoxyglucose positron-emission tomography) but suggest that Lac tends to accumulate in known areas of hypoxia/ischemia (3, 28, 29). In the aforementioned tumor studies, spectral editing techniques were not used to separate Lac from lipids nor was oxygen tension quantified independently. Several MRS animal-model studies of tumors have been conducted to investigate the relationships between ^{1}H metabolite signal intensities and such physiologic parameters as perfusion and response to radiotherapy (30−32). Relevant aspects of these studies are addressed in the Discussion section.

The objectives of this study were to measure the spectral intensities of total Cho, Cr, and Lac in vivo in human head and neck lymph node metastases and to investigate whether these measurements allow for differentiation between pretreated lymph node metastasis and normal muscular tissue and for assessment of tumor oxygenation. Although some of these aims may be achieved via ^{31}P MRS, the efficacy of the approach is still not conclusive; a 16-fold loss of signal-to-noise ratio (S/N) is suffered because of the low sensitivity of the ^{31}P nucleus (33, 34). The technical issues that were addressed in this study include the separation of large amounts of lipids from Lac in a region of the body prone to motion. Oxygenation status was measured independently using the Eppendorf polarographic oxygen electrode.

Clinical parameters

Patient Number	Age	Press Volume (cc)	Primary Site
1	48	8	R. pyriform sinus
2	50	4.8	R. tonsil
3	71	3.4	R. base of tongue
4	55	4.5	R. base of tongue
5	72	20.6, 4.1*	L. supraglottis
6	50	8	L. pyriform sinus
7	58	5.1	L. base of tongue
8	59	1.4	L. pyriform sinus
9	65	4.1	Epiglottis
10	40	2.0	L. base of tongue
11	58	3.4	Epiglottis
12	61	5.1	Base of tongue
13	58	4.5	Tonsil
14	74	1.6	Base of tongue

* Two concentric volumes were scanned. The larger volume was used for statistical calculations.

Methods

Patient Population

Fourteen men, ranging in age from 40 to 74 years (mean age, 59 years), with cytologically proved metastases of primary occurrences of squamous cell carcinoma, determined by fine-needle biopsy, were studied before undergoing treatment (see Table 1). A criterion for inclusion was a palpable node of at least 1-cm diameter visible by conventional T2-weighted MR imaging. MR imaging and MRS were performed in six healthy volunteers who served as control subjects. All studies were approved by the Stanford University Institutional Review Board, and informed consent was obtained according to the Helsinki Declaration II.

MRS Measurements

Volume-localized spectral editing was achieved using a J-difference technique that incorporates two inversion (BASING) pulses into the point-resolved spectroscopy (PRESS) excitation sequence (Fig 1), as previously described (13, 35, 36). Briefly, separation of Lac from overlapping singlets is achieved by placing the Lac methine quartet (4.1 ppm) within the BASING inversion band for Cycle 1 of the two-cycle scheme. For Cycle 2, the BASING inversion band is shifted downfield of the Lac quartet. With the time separation ($\Delta\ t_{BAS}$) between the two BASING pulses set to $\Delta t_{BAS} = 1/(2J)$ and for $TE = 1/J$, addition of Cycle 1 and Cycle 2 excitations yields the singlets, including Cho and Cr, whereas subtraction (Cycle 1 − Cycle 2) yields the Lac methyl doublet. The bandwidth of the maximum phase BASING pulses was sufficiently narrow to allow for simultaneous acquisition of the Lac doublet (1.3 ppm) and edited singlets upfield and including Cho (3.2 ppm).

Data were collected at 1.5 T using a General Electric Echo-Speed system (G.E. Medical Systems, Milwaukee WI) equipped with self-shielded gradients (maximum magnitude, 2.2 G/cm; maximum slew rate, 12 G/cm/millisecond). Acqui-

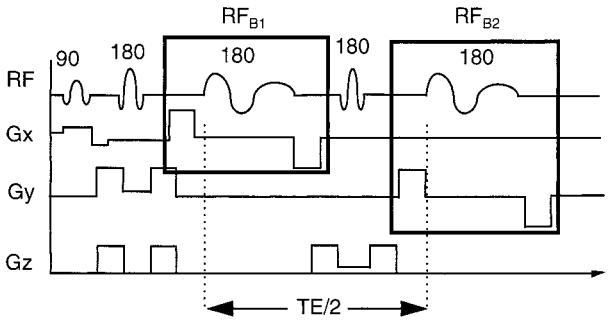

FIG 1. Dual BASING with PRESS excitation. The two BASING pulses (RF_{B1} and RF_{B1}) are separated in time by TE = 2 msec. For Cycle 1, the Lac methine quartet is included in the BASING inversion band, whereas for Cycle 2, the BASING center frequency is shifted downfield to exclude all metabolites of interest. The addition of Cycle 1 and Cycle 2 spectra yields the singlets, whereas the subtraction of Cycle 2 from Cycle 1 yields the Lac methyl doublet.

sition was with a four-element head, neck, and cervical phased-array coil (MRI Devices Corp., Waukesha, WI) operating in receive-only mode (the body coil was used to transmit). The receive coil provided uniform coverage of both the head and neck regions, with a measured S/N that was comparable with the S/N offered by the G.E. quadrature birdcage head coil, albeit over approximately twice the volume. Phantom measurements showed that the reconstructed SI deviated by 10% or less across the relevant coil regions that included the neck nodes studied.

To help localize the lesion for the MRS acquisition, T1-weighted spin-echo (500/8/2 [TR/TE/excitations]; field of view, 21 cm; matrix, 256 × 160) and dual spin-echo proton density–/T2-weighted (3000/14/84/2 [TR/first TE/second TE/excitations]; field of view, 21 cm; matrix = 256 × 160) images were first acquired. The PRESS volume was prescribed in an attempt to encompass as much of the T2-enhancing lesion as possible. The average prescribed volume was 5.5 cc and ranged from 1.4 to 20.6 cc (see Table 1).

After shimming, using first-order corrections, the MRS data (2/144 [TR/TE]) were then acquired with a receiver bandwidth of 1250 Hz (512 points). Three minimum-phase CHESS pulses of 60 Hz bandwidth were used for water suppression (37, 38). For most patients, 256 excitations were acquired, yielding an MRS study time of approximately 8.5 min. The MRS acquisition time was doubled for two patients with small nodes. Unsuppressed spectra (2000/38/16) to obtain water references were acquired from all except three patients. For four patients, an additional MRS data set was acquired from a region that comprised neck muscle tissue. The MRS data acquired from the volunteers were localized solely to muscle tissue. The overall examination time, including patient positioning, localization, shimming, and MRS acquisition, was approximately 1 hour.

MRS Processing

The accumulated free induction decays were processed and displayed using software written by the authors for the Matlab (The Mathworks Inc., Natick, MA) and Idl (Research Systems Inc., Boulder, CO) platforms. To allow for comparison of absolute spectral intensities, the phased-array data from each patient were normalized by the PRESS volume and receiver gain and combined in a manner designed to maximize the final S/N (39). The transmitter gain was not used to correct the SI (40) because the loading factor would have to be determined from the body coil rather than the receive coils. Regardless, this would not have been a significant factor because, for all patients, the SD of the transmitter gain was only 4% of the mean.

To reduce errors resulting from motion, a phase regularization algorithm was developed to lessen the deleterious effects of shot-to-shot phase variations and to restore the original metabolite SI (13, 41). Briefly, each individual free induction decay of the data set was zero-filled to 1024 points, apodized with a 12-Hz line-broadening window, and Fourier transformed; a zero-order phase correction factor was determined using the lipid CH_2 peak (nominally 1.3 ppm) as a reference. After the phase factors from each Cycle 1 and Cycle 2 acquisition of a given experiment were determined, the data were reprocessed with a 2-Hz line-broadening window and phased using the correction factors determined from the 12-Hz apodization. The data were then either summed or subtracted to generate either the uncoupled or coupled spectra. Two patients did not have sufficient lipid signals to allow for automatic phasing and, in those instances, the regularization algorithm was not used.

To help quantify the lipid cancellation errors that remained after processing, an ''error'' spectrum was generated by subtracting phased adjacent Cycle 1 acquisitions from each other and adjacent Cycle 2 acquisitions from each other and summing the result. The overall noise variance for the Lac peak was determined by integrating the respective peak area in the error spectrum, squaring it, and adding the result to the random noise variance.

Peak areas assigned to Cho and Cr were calculated by numerically integrating the uncoupled (summed) spectra within the 13-Hz windows of 3.3 to 3.1 ppm and 3.1 to 2.9 ppm, respectively. Lac and lipid peak areas were calculated by numerically integrating the respective coupled and uncoupled spectra from 1.5 to 1.1 ppm (26 Hz). The range of integration for the water peak was 5.4 to 4.0 ppm. The uncoupled spectra were baseline-corrected by fitting a line to points surrounding the peaks of interest and subtracting the fitted result. The coupled (difference) spectra were baseline corrected by removing only the DC offset to avoid altering or masking any cancellation artifacts that may have resulted from lipid contamination.

Metabolite:water ratios were calculated by dividing the volume-normalized metabolite signal intensities by the TE = 38 msec water SI. For the three patients who did not undergo water imaging, the mean water value from the other 11 patients was used. A Pearson's correlation coefficient was calculated to relate both volume-normalized metabolite SI and metabolite/water SI to pO_2. Student's *t* test was used to compare metabolite signal intensities between nodes with oxygen levels less than and greater than 10 mm Hg, which may be a reliable cutoff that indicates increased resistance to radiotherapy (15). Comparisons were also made between node and muscle tissue.

Oxygen Tension Measurements

Tumor oxygenation was measured with the Eppendorf pO_2 Histograph (Eppendorf, Hamburg, Germany), a computerized polarographic needle electrode system. Detailed descriptions of the procedure have been published previously (18). In summary, a gold microcathode (12-μm diameter) embedded in a stainless steel shaft was polarized against a silver-silver chloride anode placed on the skin of the patient. The resulting current (4−5 pA/mm Hg) was proportional to the oxygen partial pressure in the tissue. Calibration was done before and after measurements by using a phosphate-buffered saline solution equilibrated with air or 100% nitrogen. The values were corrected for barometric pressure and body temperature. The skin was anaesthetized, and a 20-gauge plastic trocar was inserted. The probe was inserted through the trocar into the tissue and moved automatically in a stepwise pattern of 0.7 mm forward and then by 0.3 mm backward to prevent pressure artifact. Each track consisted of 20 samples. Two tracks were recorded in normal subcutaneous tissues of the neck, and then two or three independent tracks were recorded in the tumor. A complete measurement session took 20 to 30 minutes and was

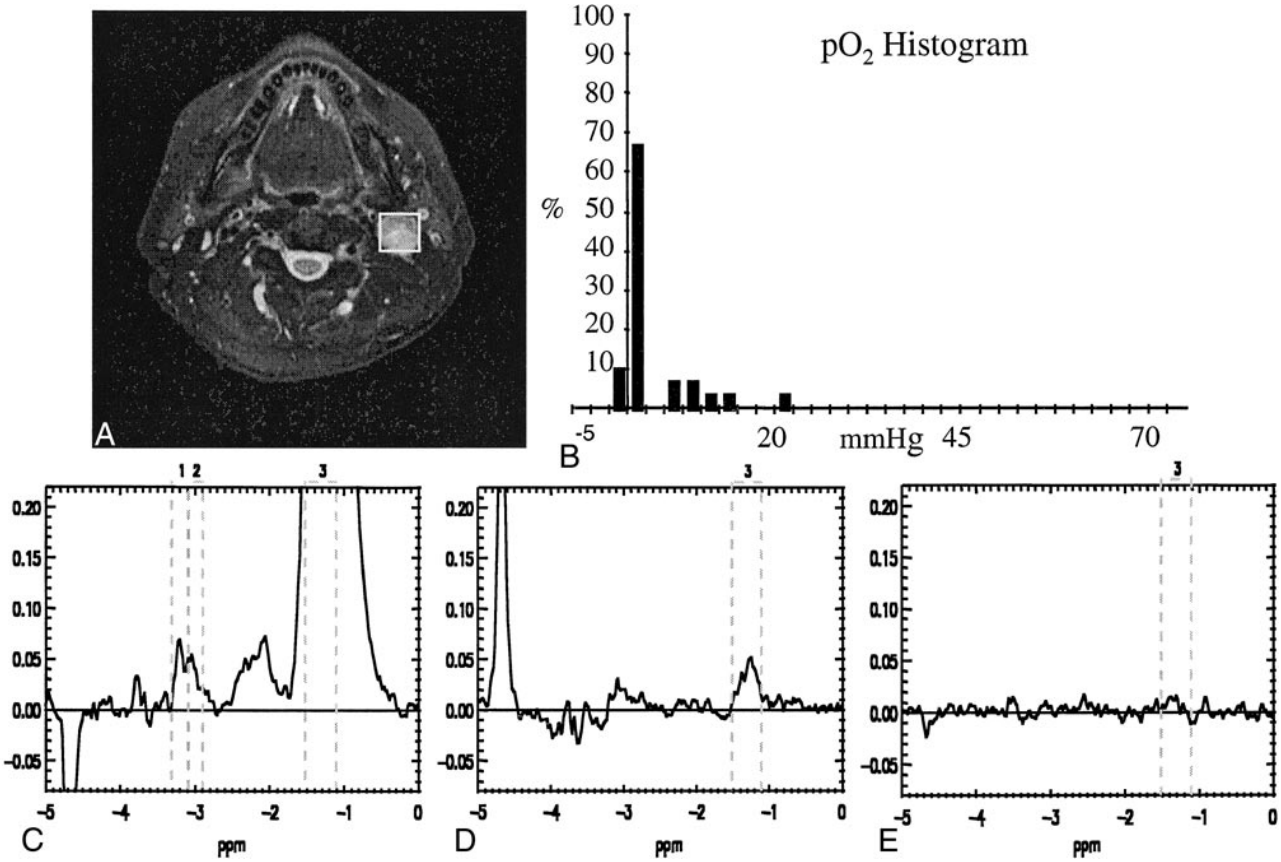

FIG 2. Data from a representative hypoxic node in patient 7.
A, T2-weighted image (3000/85/2) shows the location of the PRESS box.
B, Histogram of oxygenation measurements. The median pO_2 value is 1.3 mm Hg, which is very suggestive of hypoxia.
C, Uncoupled (Cycle 1 + Cycle 2).
D, Coupled (Cycle 1—Cycle 2).
E, Error spectra acquired with MRS parameters of 2000/144/256. The Cho:Cr ratio is 1.3.

usually tolerated well by the patients. There were no significant complications. For each patient, a pO_2 histogram with bin widths equal to 2.5 mm Hg was generated. A median pO_2 value was also calculated. To ensure that the electrode measurements would not affect MR results, the oxygenation measurement procedure was performed after MR imaging.

Results

The short TE = 38 msec MRS water intensities were extremely well correlated with PRESS volume ($r = 1.00$) so that, after volume normalization, the SD of the water SI was only 17% of the overall mean. This uniformity indicated that water relaxation times and coil reception profiles were relatively homogeneous and resulted in the volume-normalized metabolite (Cho, Cr, Lac) signal intensities also being well correlated ($r = .92$, $r = .96$, $r = .96$) with the respective metabolite:water ratios.

Figure 2 shows spectra and a pO_2 histogram from a representative hypoxic node (patient 7, median $pO_2 = 1.3$ mm Hg). The uncoupled spectrum (Fig 2C) exhibits distinct Cho and Cr peaks with a Cho:Cr ratio of 1.3 that is elevated compared with that of the muscle spectra. The difference spectrum (Fig 2D) contains a peak centered at 1.3 ppm, presumed to be Lac, that was a factor of five greater than the computed error signal (Fig 2E). Accounting only for random noise, the S/N of Cho, Cr, and Lac were 38:1, 28:1, and 45:1, respectively.

Data from another hypoxic node (patient 1, median $pO_2 = 0.71$ mm Hg) are shown in Figure 3. Again, the Cho:Cr ratio is elevated (Fig 3C) and a Lac signal is evidenced in the difference spectrum (Fig 3D). Although there were not sufficient lipids in this acquisition to implement the phase regularization algorithm, the error signal was still minimal (Fig 3E). It remains possible, however, that the metabolite signals were underestimated because of motion-induced phase variations (41), which may partly account for the Lac intensity being approximately 60% of that for patient 7. A further distinction is that the Cho signal for patient 1 (Fig 3C) is more elevated, whereas Cr is reduced. This resulted in a Cho:Cr ratio of 4.3, which was more than a factor of three greater than that for patient 7.

Spectra and a pO_2 histogram from a more aerobic node (patient 2, median $pO_2 = 14.1$ mm Hg) are shown in Figure 4. Singlet resonances in the Cho region are visible (Fig 4C), and the Cho:Cr ratio was 3.9. The difference spectrum (Fig 4D)

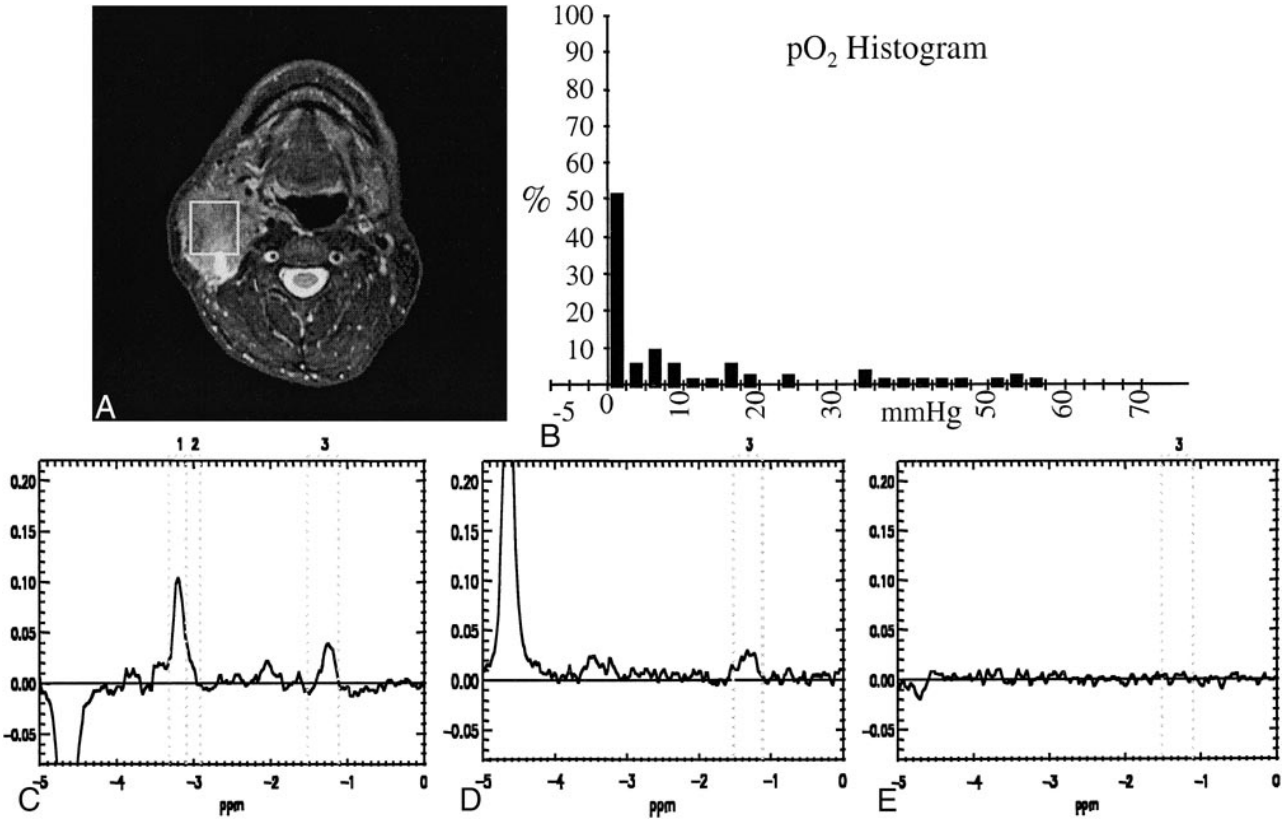

FIG 3. Data from a hypoxic node in patient 1.
A, T2-weighted image (3000/85/2) shows the location of the PRESS box.
B, Histogram of oxygen measurements. The median pO_2 value is 0.7 mm Hg.
C, Uncoupled (Cycle 1 + Cycle 2).
D, Coupled (Cycle 1—Cycle 2).
E, Error spectra acquired with MRS parameters of 2000/144/256. The Cho:Cr ratio is 4.3.

shows no distinct Lac resonance. The error spectrum (Fig 4E) does contain more signal energy in the 1.3 ppm region than for patient 7. This was reflective of an increased amount of random noise associated with the image for patient 2.

A representative muscle spectrum is shown in Figure 5 and displays a Cho:Cr ratio of 0.48, which is significantly less than that of the nodes. Although there were large amounts of lipids, the Lac value was negligible and was indistinguishable from the noise baseline. A lipid suppression factor of 3471 was measured by dividing the uncoupled signal (Fig 5B) by the coupled (Fig 5C) signal. For all muscle images, the average lipid S/N was 2954 and the average lipid suppression factor was 787. Overall, the lipid signals were 3.2 times higher in muscle tissue than in the nodes, where the average lipid:Lac ratio was measured to be 36. This would indicate that a singlet suppression factor of 787, if it were achieved in the nodes, would be more than adequate.

The accumulated Lac measurements are shown in Figure 6. A linear fit (Fig 6A) showed a moderately negative correlation ($r = -.74$) between volume normalized Lac SI and pO_2. A similar coefficient ($r = -.76$) was found between Lac:H_2O ratios and pO_2 (Fig 6B). Visual inspection of the plots indicates that Lac SI may level off above oxygen tensions of 15 mm Hg, but more data are needed at these higher values for confirmation. Figure 6C shows box and whisker plots of Lac SI for three data groupings ($pO_2 < 10$ mm Hg, $pO_2 \geq 10$ mm Hg, muscle). There was a statistically significant differentiation between all three groups ($P < .05$). Lac SI was approximately twice as high for oxygen levels less than 10 mm Hg than for oxygen values greater than or equal to 10 mm Hg ($P = .01$). Overall, Lac was significantly higher in cancer than in muscle ($P = .01$).

Magnitude Lac SI was not correlated with lipid SI ($r = .18$), further indicating that the overall amount of lipid contamination may have been minimal. There was no correlation between PRESS volume and pO_2 ($r = -.05$), which is inconsistent with some previous measurements comparing oxygenation and node volume (20, 42). PRESS volume and Lac SI also were not correlated ($r = .16$).

Summary singlet (Cho, Cr) data are shown in Figure 7. The mean Cho:Cr ratio in the nodes was 2.9 ± 1.6, which was 5.3 times higher ($P = .0006$) than that in muscle, where the ratio was $.55 \pm .21$ (Fig. 7D). Cho SI was not well correlated with pO_2 ($r = -.43$) (Fig 7A and B), and there was not a statistically significant differentiation between

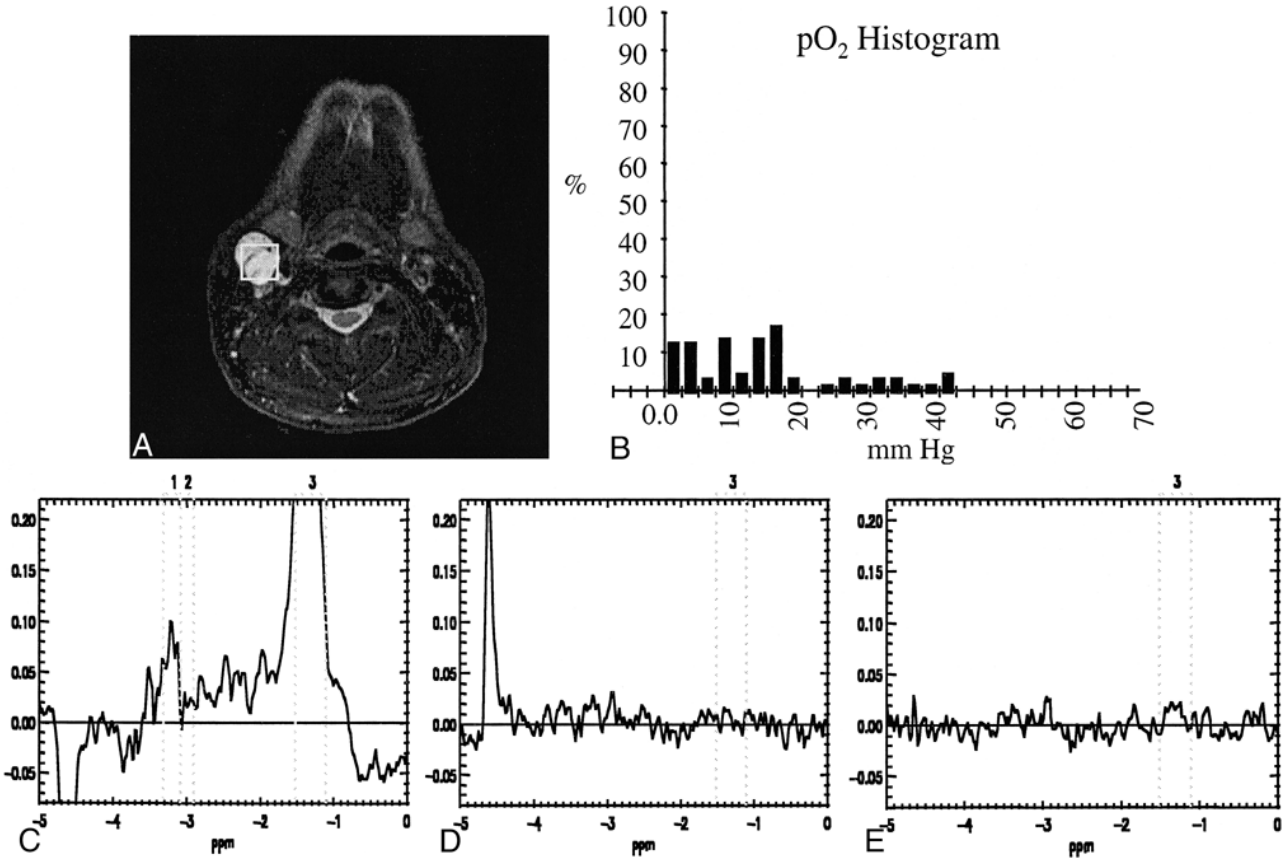

FIG 4. Data from a more aerobic node in patient 2.

A, T2-weighted image (3000/85/2) shows the location of the PRESS box.

B, Histogram of oxygen measurements. The median pO_2 value is 14.1 mm Hg, which is more aerobic than the median values for patients 1 and 7.

C, Uncoupled (Cycle 1 + Cycle 2).

D, Coupled (Cycle 1—Cycle 2).

E, Error spectra acquired with MRS parameters of 2000/144/256. The Cho:Cr ratio is 3.9.

nodes with oxygenation pressures less than and greater than 10 mm Hg (Fig 7C). Of note, two nodes with the lowest Cho signal intensities had median oxygenation pressures that averaged to 27.6 mm Hg. More measurements are required to determine whether this represents a distinct trend toward reduced Cho levels at higher pressures.

Discussion

The technical difficulties associated with measuring coupled and uncoupled ^1H spin signals in the human neck are substantial. Artifacts arising from motion and other instabilities, particularly in the presence of high lipid concentrations, can corrupt metabolite intensity measurements. Shimming can be difficult because of local susceptibility differences, and localization may be compromised when using a PRESS-based sequence, which allows for the prescription of only rectangular volumes of interest that, most likely, will not exactly encompass the lesion. Despite these and other difficulties, it seems that several trends have emerged that may provide impetus for further investigations.

The results show that there was a significant increase in Cho:Cr ratios in lymph node metastases of squamous cell carcinoma as compared with normal muscle tissue. The increased ratios resulted more from a decline of the Cr signal than from an elevation of Cho. Of note is that the mean Cho:Cr value of 2.9 was 71% higher than the in vivo Cho:Cr ratio of 1.7 reported by Mukherji et al (9) in primary sites at similar echo and pulse repetition times (136/2000). This may reflect that there is less residual Cr in lymph nodes compared with the more muscular tongue base. Differing amounts of local necrosis could also account for the ratio dissimilarities. Cho levels could also be elevated in immunostimulated nodes, thus contributing to the ratio increase, although it should be noted that an in vitro study of resected nodal tissue (43) showed that Cho:Cr ratios seemed to be similar in both normal and immunostimulated nodes. Another relevant factor in comparing the results from the study of primary sites (9) with those of the current study of metastasis could be the different processing algorithms implemented to estimate signal intensities. Mukherji et al (9) used a gaussian fit to estimate

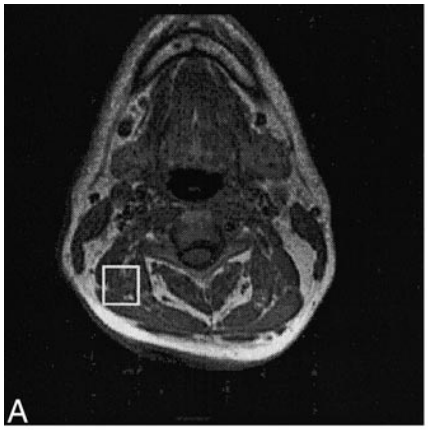

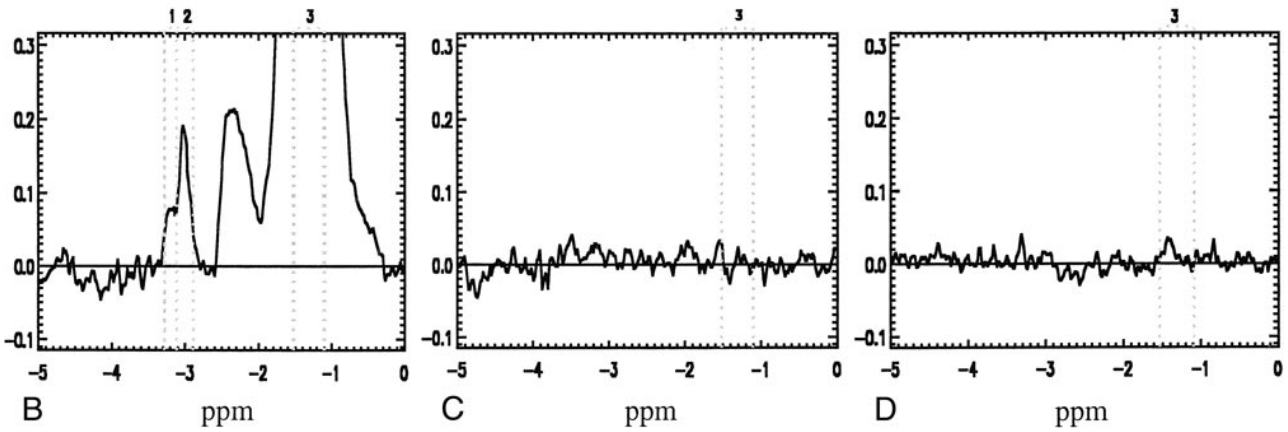

FIG 5. Representative muscle spectrum. *A,* T1-weighted image (500/8/2) from a normal volunteer shows the location of the PRESS box enclosing muscle tissue.
B, Uncoupled (Cycle 1 + Cycle 2).
C, Coupled (Cycle 1—Cycle 2).
D, Error spectra acquired with MRS parameters of 2000/144/256. The Cho:Cr ratio is 0.48, and the lipid suppression factor is greater than 3000.

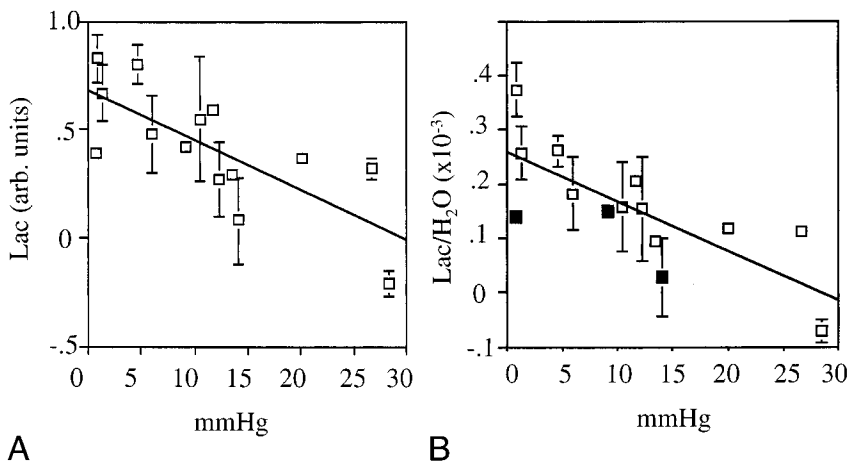

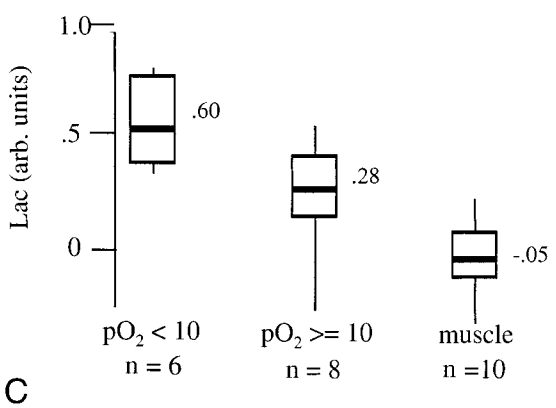

FIG 6. Accumulated Lac measurements.
A, Scatter plot of Lac SI versus pO_2. The *error bars* are the SD after including the computed error signal (see Fig 2C). A linear fit yielded a Pearson's correlation coefficient of −0.74.
B, Scatter plot of Lac/H_2O versus pO_2. The Pearson's coefficient is −0.76. The average water signal was used for normalizing the three samples with *darkened boxes.*
C, Box and whiskers plot for three data groups: $pO_2 < 10$ mm Hg, $pO_2 \geq 10$ mm Hg, and muscle. All three groups are statistically different ($P < 0.05$). The mean values for each group are annotated (0.60, 0.28, −0.05). The *boxes* span the range of Lac signal intensities from the 25th to 75th percentiles. The *bars* within the *boxes* denote the median value, whereas the *vertical lines* ("whiskers") are reflective of the data range.

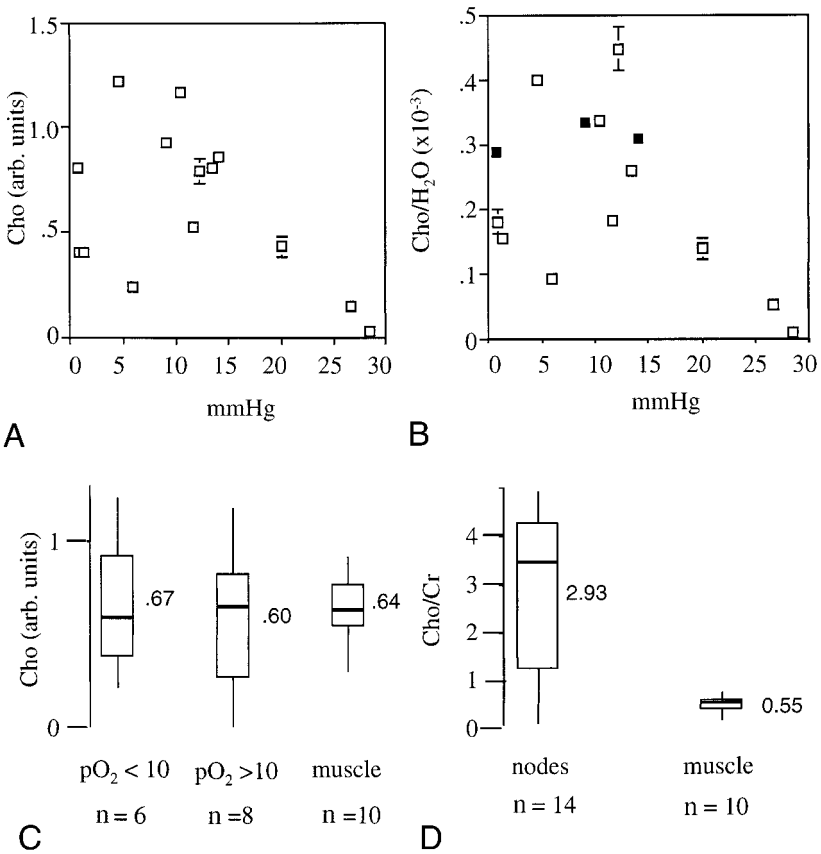

FIG 7. Accumulated Cho and Cr measurements.

A, Scatter plots of Cho SI versus pO2.

B, Scatter plots of Cho/H_2O SI versus pO_2. The correlation coefficients are −0.43 and −0.45, respectively. The average water signal was used for normalizing the three samples *darkened black boxes.*

C, Box and whiskers plots of Cho SI for three data groups: pO2 < 10 mm Hg, pO2 ≥ 10 mm Hg, and muscle. The mean Cho values are annotated, and the data were not statistically different.

D, Box and whiskers plots of Cho:Cr ratios show statistically significant differentiation between muscle and cancer. The mean values are annotated.

peak areas, whereas, for this study, numerical integration was used. Numerical integration was deemed more practical because the Cho peak can comprise several moieties, including carnitine and various Cho-containing compounds (1) and, often, distinct Cho and Cr peaks were not identifiable (see, for example, Fig 4C).

The data strongly suggest that Lac is present in metastatic occurrences of human squamous cell carcinoma. This is consistent with the fact that tumor oxygenation, like tumor microcirculation, is compromised and that median pO_2 values in neck nodes have been shown to be significantly lower than those in healthy tissue (44). The MRS data also suggest that Lac SI is negatively correlated with oxygenation tension over the measured range spanning approximately 0 to 30 mm Hg. Although it is not clear that the relationship is, or should be, linear because of the complicated interplay of many factors, there is evidence that Lac SI measurements may aid in discriminating between nodes with oxygen tensions less than 10 mm Hg and those with oxygen tensions greater than 10 mm Hg. As shown by Wouters and Brown (45), assessing the population of cells at these more intermediate oxygen values, rather than determining radiobiological hypoxic fraction, may be most important in predicting tumor response to fractionated radiotherapy.

Because of the wide range of oxygen values measured, it may be difficult to compare our results with those from previous MRS studies that used animal models (30−32), in which oxygen pressures are lower and ranges are more restricted. That oxygenation is significantly reduced in animal models was confirmed by a recent study of 12 transplanted tumors; it was shown that the median pO_2 was only 10% that of the pooled human data (46). Animal tumors, regardless of hypoxic fraction, tended to have median pO_2 values in the 1- to 3-mm Hg range, whereas, for most human tumors, the median was above 10 mm Hg. In our study, the average of the median pO_2 pressures was 11.4 ± 8.9 mm Hg, which is consistent with previously published results for metastatic neck nodes (44).

A study comparing perfusion and Lac SI measurements in a C6 glioma model (31) illustrates the potential difficulties in extrapolating results from the more hypoxic animal tumors to human cancers. The authors measured a putative perfusion threshold of 5 mL/100 g/minute above which Lac SI remained constant. This led to a low overall correlation between perfusion and Lac SI. Of note is that perfusion values ranged from only 4.8 to 20.8 mL/100 g/minute, all of which are lower than the mean flow of 24 ± 19 mL/100 g/minute previously measured in human metastatic neck cancer (47). Considering that gliomas have median pO_2 values of approximately 2 mm Hg (44), it was unlikely that any samples had oxygen tensions above 10 mm Hg. The results from this study suggest that Lac levels in the C6 glioma model may again begin to decline at higher oxygen tensions than were measured.

A recent animal study (32) showed that baseline Lac levels were similar in the EMT6 and RIF1 tumors, although the RIF1 tumor has a lower hypoxic fraction as measured by single radiation doses (48). This similarity in Lac signal intensities between models is not inconsistent with our results because the median oxygen tension of the RIF1 model is still not very high and also on the order of 2 mm Hg (46). Previous studies also have shown difficulties in distinguishing between such types of tumors with an Eppendorf probe (49). If it is confirmed that hypoxic fraction is not the best measure to predict tumor response in humans (especially to fractionated radiotherapy) (45) and that an oxygenation delineation of 10 mm Hg could be of important prognostic value (15), then the relevance of some aspects of the animal models may be called into question. Nevertheless, it should be noted that the results from this study do not obviate the conclusion from the EMT6/RIF1 studies that the ability to measure Lac SI may lead to improved means of monitoring treatment (32). Confirmation in humans, however, is required.

An interesting aspect of an MRS study of RIF1 tumors subject to blood flow modifiers (30) was that Cho SI diminished when perfusion was increased by the administration of nicotinamide. This was hypothesized to have resulted from a decline in the breakdown of phosphatidylcholine to glycerophosphorylcholine and ultimately to Cho and phosphorylcholine. In our study, although there was a low overall negative correlation between Cho SI and pO_2, there seemed to be a notable Cho SI decline at very high oxygen values ($>$20 mm Hg). It will be important to investigate further and verify these reduced Cho levels, both for helping to determine oxygenation and because there is a danger that the sensitivity of MRS in detecting head and neck cancer could be compromised if the Cho SI drops too much.

To determine the relationship between metabolite SI and tumor oxygenation better, future investigations, with possibly improved acquisition and processing strategies, are required. Despite the high singlet suppression factors measured in muscle and the lack of correlation between absolute lipid and Lac signal intensities in the nodes, it is impossible to rule out that lipids or other signals did not corrupt Lac measurements. Consequently, it may be prudent to investigate single-shot singlet suppression techniques such as multiple quantum filters (50), although a penalty of a factor of two loss of Lac S/N would be incurred. Another source of error in the Lac measurement may have resulted from contamination by the neighboring alanine resonance (1.5 ppm), which has been detected in vitro in extracts of head and neck cancer (9) and which has coupling properties similar to those of Lac. Considering that alanine will pass through the J-difference filter, the Lac SI may have been overestimated. Even though alanine SI may be correlated with Lac SI, because both are redox partners of pyruvate, it would still be useful to separate the two signals. This may require implementing improved higher-order shimming techniques and imaging at higher fields to achieve finer chemical-shift resolution.

Another issue that may need to be addressed concerns non-uniform metabolite distributions, as have been previously observed in studies of brain tumors (51). It is unknown to what extent head and neck lesions are also spatially heterogeneous, not withstanding the fact that Eppendorf measurements suggest that oxygenation may be relatively uniform throughout the lesion (42). In this study, patient 6, who had a very large node, underwent imaging twice with two concentric PRESS volumes equal to 20.6 and 4.1 cc, respectively. Although it is impossible to generalize from this one case, the metabolite signal intensities of the two volumes were similar. To assess tumor heterogeneity better, further investigations using chemical-shift imaging techniques (52, 53) will likely be required, as will improved phase-array coils, to enhance the S/N and resolution. Finally, it would be useful to attempt absolute metabolite quantification, which will mandate measurement of both water and metabolite relaxation times.

An alternative approach to assessing blood flow and oxygenation is to measure T_2* changes via gradient-echo MR imaging or spectroscopic imaging of water (54, 55). Because previous studies mainly have observed changes of signal as a result of the administration of vasomodulators such as carbogen, future technical advances may still be required to enable absolute quantification. Eventually, MR imaging of the water signal may be combined with a ^{1}H MRS examination to offer a more comprehensive study. In particular, perfusion measurements may be helpful in differentiating regions of active tumor from regions of local necrosis, where Lac also can collect. ^{31}P MRS also may offer important information despite its low sensitivity. Other noninvasive MR techniques for assessing oxygenation, such as ^{19}F MRS of hypoxia binding nitro imidazoles (56) or ^{19}F T1 measurements of artificial blood substitutes (57), hold promise but have not yet been tested on humans.

The results of this study point to a potential clinical role for ^{1}H MRS for staging and monitoring treatment of head and neck cancer. An important goal of future investigations is to determine whether ^{1}H MRS offers sufficient specificity to differentiate between metastatic and enlarged reactive nodes. If confirmed, then ^{1}H MRS may be used to monitor post-treatment recurrence and intratreatment response. If it is confirmed that metabolite signal intensities can help in the assessment of oxygenation status, then ^{1}H MRS may also be useful in staging treatment.

Conclusion

Cho:Cr ratios and Lac signal intensities were increased in pretreated lymph node metastases of

squamous cell carcinoma relative to muscle tissue, and Lac (and, to a lesser extent, Cho) signal intensities were reflective of tissue oxygenation status. These results indicate that future in vivo investigations, which may require implementation of improved localization techniques, are warranted and should be geared to assessing the clinical utility of ^{1}H MRS in helping to stage and monitor therapy.

Acknowledgments

This work was supported by National Institutes of Health grants CA 48269, RR-09784, and CA 67166–01. The authors are grateful to Jackie Itnyre for help with the management of patient data and Sherie Budenz for help coordinating the patient studies. The authors also thank G.E. Medical Systems for their support.

References

1. Evanochko WT, Sakai TT, Ng TC, et al. **NMR study of in vivo RIF-1 tumors: analysis of perchloric acid extracts and identification of 1H, 31P and 13C resonances.** *Biochim Biophys Acta* 1984;805:104–116
2. Langkowski JH, Wieland J, Bomsdorf H, et al. **Pre-operative localized in vivo proton spectroscopy in cerebral tumors at 4.0 tesla: first results.** *Magn Reson Imaging* 1989;7:547–555
3. Alger JR, Frank JA, Bizzi A, et al. **Metabolism of human gliomas: assessment with H-1 MR spectroscopy and F-18 fluorodeoxyglucose PET (comment).** *Radiology* 1990;177:633–641
4. Bruhn H, Frahm J, Gyngell ML, et al. **Noninvasive differentiation of tumors with use of localized H-1 MR spectroscopy in vivo: initial experience in patients with cerebral tumors.** *Radiology* 1989;172:541–548
5. Arnold DL, Shoubridge EA, Villemure JG, Feindel W. **Proton and phosphorus magnetic resonance spectroscopy of human astrocytomas in vivo: preliminary observations on tumor grading.** *NMR Biomed* 1990;3:184–189
6. Negendank W. **Studies of human tumors by MRS: a review.** *NMR Biomed* 1992;5:303–324
7. Castillo M., Kwock L, Mukherji SK. **Clinical applications of proton MR spectroscopy.** *AJNR Am J Neuroradiol* 1996;17: 1–15
8. Leach MO. **Introduction to in vivo MRS of cancer: new perspectives and open problems.** *Anticancer Res* 1996;16:1503–1514
9. Mukherji SK, Schiro S, Castillo M, Kwock L, Muller KE, Blackstock W. **Proton MR spectroscopy of squamous cell carcinoma of the extracranial head and neck: in vitro and in vivo studies.** *AJNR Am J Neuroradiol* 1997;18:1057–1072
10. Mukherji SK, Schiro S, Castillo M, et al. **Proton MR spectroscopy of squamous cell carcinoma of the upper aerodigestive tract: in vitro characteristics.** *AJNR Am J Neuroradiol* 1996;17: 1485–1490
11. van Zijl P, Moonen CT, Gillen J, et al. **Proton magnetic resonance spectroscopy of small regions (1 mL) localized inside superficial human tumors: a clinical feasibility study.** *NMR Biomed* 1990;3:227–232
12. Adalsteinsson E, Spielman DM, Pauly JM, Terris DJ, Sommer G, Macovski A. **Feasibility study of lactate imaging of head and neck tumors.** *NMR Biomed* 1998;11:360–369
13. Star-Lack J, Spielman D, Adalsteinsson E, Kurhanewicz J, Terris DJ, Vigneron DB. **In vivo lactate editing with simultaneous detection of choline, creatine, NAA, and lipid singlets at 1.5 T using PRESS excitation with applications to the study of brain and head and neck tumors.** *J Magn Reson* 1998;133:243–254
14. Gatenby RA, Kessler HB, Rosenblum JS, et al. **Oxygen distribution in squamous cell carcinoma metastases and its relationship to outcome of radiation therapy.** *Int J Radiat Oncol Biol Phys* 1988;14:831–838
15. Brizel DM, Sibley GS, Prosnitz LR, Scher RL, Dewhirst MW. **Tumor hypoxia adversely affects the prognosis of carcinoma of the head and neck.** *Int J Radiat Oncol Biol Phys* 1997;38: 285–289
16. Nordsmark M, Overgaard M, Overgaard J. **Pretreatment oxygenation predicts radiation response in advanced squamous cell carcinoma of the head and neck.** *Radiother Oncol* 1996;41: 31–39
17. Brown JM, Giaccia AJ. **The unique physiology of solid tumors: opportunities (and problems) for cancer therapy.** *Cancer Res* 1998;58:1408–1416
18. Vaupel P, Schlenger K, Knoop C, Hockel M. **Oxygenation of human tumors: evaluation of tissue oxygen distribution in breast cancers by computerized O_2 tension measurements.** *Cancer Res* 1991;51:3316–3322
19. Nordsmark M, Bentzen SM, Overgaard J. **Measurement of human tumour oxygenation status by a polarographic needle electrode: an analysis of inter- and intratumour heterogeneity.** *Acta Oncol* 1994;33:383–389
20. Terris DJ, Dunphy EP. **Oxygen tension measurements of head and neck cancers.** *Arch Otolaryngol Head Neck Surg* 1994;120: 283–287
21. van der Sprenkel JWB, Luyten PR, Van Rijen PC, Tulleken CA, Den Hollander JA. **Cerebral lactate detected by regional proton magnetic resonance spectroscopy in a patient with cerebral infarction.** *Stroke* 1988;19:1556–1560
22. Bruhn H, Frahm J, Gyngell ML, Merboldt KD, Hanicke W, Sauter R. **Cerebral metabolism in man after acute stroke: new observations using localized proton NMR spectroscopy.** *Magn Reson Med* 1989;9:126–131
23. Groenendaal F, Veenhoven RH, van der Grond J, Jansen GH, Witkamp TD, de Vries LS. **Cerebral lactate and *N*-acetyl-aspartate/choline ratios in asphyxiated full-term neonates demonstrated in vivo using proton magnetic resonance spectroscopy.** *Pediatr Res* 1994;35:148–151
24. Warburg O. **On the origin of cancer cells.** *Science* 1956;123: 309–314
25. Kallinowski F, Vaupel P, Runkel S, et al. **Glucose uptake, lactate release, ketone body turnover, metabolic micromilieu, and pH distributions in human breast cancer xenografts in nude rats.** *Cancer Res* 1988;48:7264–7272
26. Schupp DG, Merkle H, Ellerman JM, Ke Y, Garwood M. **Localized detection of gliomay glycolysis using edited ^{1}H MRS.** *Magn Reson Med* 1993;30:18–27
27. Veech RL. **The metabolism of lactate.** *NMR Biomed* 1991;4: 53–58
28. Herholz K, Heindel W, Luyten PR, et al. **In vivo imaging of glucose consumption and lactate concentration in human gliomas.** *Ann Neurol* 1992;31:319–327
29. Go KG, Kamman RL, Mooyaart EL, et al. **Localized proton spectroscopy and spectroscopic imaging in cerebral gliomas, with comparison to positron emission tomography.** *Neuroradiology* 1995;37:198–206
30. Bhujwalla ZM, Shungu DC, Glickson JD. **Effects of blood flow modifiers on tumor metabolism observed in vivo by proton magnetic resonance spectroscopic imaging.** *Magn Reson Med* 1996;36:204–211
31. Terpstra M, High WB, Luo Y, de Graaf RA, Merkle H, Garwood M. **Relationships among lactate concentration, blood flow and histopathologic profiles in rat C6 glioma.** *NMR Biomed* 1996;9: 185–194
32. Aboagye EO, Bhujwalla ZM, He Q, Glickson JD. **Evaluation of lactate as a ^{1}H nuclear magnetic resonance spectroscopy index for noninvasive prediction and early detection of tumor response to radiation therapy in EMT6 tumors.** *Radiat Res* 1998; 150:38–42
33. McKenna WG, Lenkinski RE, Hendrix RA, Vogele KE, Bloch P. **The use of magnetic resonance imaging and spectroscopy in the assessment of patients with head and neck and other superficial human malignancies.** *Cancer* 1989;64:2069–2075
34. Nordsmark M, Keller J, Nielsen OS, Lundorf E, Overgaard J. **Tumour oxygenation assessed by polarographic needle electrodes and bioenergetic status measured by 31P magnetic resonance spectroscopy in human soft tissue tumours.** *Acta Oncol* 1997;36:565–571
35. Mescher M, Tannus A, Johnson O, Garwood M. **Solvent suppression using selective echo dephasing.** *J Magn Reson A* 1996; 123:226–229
36. Star-Lack J, Nelson SJ, Kurhanewicz J, Huang LR, Vigneron DB. **Improved water and lipid suppression for 3-D PRESS CSI using RF band selective inversion with gradient dephasing (BASING).** *Mag Reson Med* 1997;38:311–321
37. Haase A, Frahm J, Hanicke W, Matthaei D. **^{1}H NMR chemical shift selective (CHESS) imaging.** *Phys Med Biol* 1985;30: 341–344

38. Webb PG, Sailasuta N, Kohler SJ, Raidy T, Moats RA, Hurd RE. **Automated single-voxel proton MRS: technical development and multisite verification.** *Magn Reson Med* 1994;169:207–212
39. Roemer PB, Edelstein WA, Hayes CE, Souza SP, Mueller OM. **The NMR phased array.** *Magn Reson Med* 1990;16:192–225
40. Soher BJ, van Zijl PC, Duyn JH, Barker PB. **Quantitative proton MR spectroscopic imaging of the human brain.** *Magn Reson Med* 1996;35:356–363
41. Zhu G, Gheorghiu D, Allen PS. **Motional degradation of metabolite signal strengths when using STEAM: a correction method.** *NMR Biomed* 1992;5:209–211
42. Lartigau E, Le Ridant AM, Lambin P, et al. **Oxygenation of head and neck tumors.** *Cancer* 1993;71:2319–2325
43. Mountford CE, Lean CL, Hancock R, et al. **Magnetic resonance spectroscopy detects cancer in draining lymph nodes.** *Invasion Metastasis* 1993;13:57–71
44. Vaupel P. **Blood flow and oxygenation status of head and neck carcinomas.** *Adv Exp Med Biol* 1997;428:89–95
45. Wouters BG, Brown JM. **Cells at intermediate oxygen levels can be more important than the "hypoxic fraction" in determining tumor response to fractionated radiotherapy.** *Radiat Res* 1997; 147:541–550
46. Adam M, Dorie MJ, Brown JM. **Oxygen tension measurements of tumors growing in mice.** *Int J Rad Oncol Biol Phys* 1999;45: 171–180
47. Wust P, Stahl H, Dieckmann K, et al. **Local hyperthermia of N2/N3 cervical lymph node metastases: correlation of technical/thermal parameters and response.** *Int J Radiat Oncol Biol Phys* 1996;34:635–646
48. Brown JM, Twentyman PR, Zamvil SS. **Response to the RIF-1 tumor in vitro and in C3H/Km mice to X-radiation (cell survival, regrowth delay, and tumor control), chemotherapeutic agents, and activated macrophages.** *J Natl Cancer Inst* 1980;64: 605–611
49. Horsman MR, Khalil AA, Siemann DW, et al. **Relationship between radiobiological hypoxia in tumors and electrode measurements of tumor oxygenation.** *Int J Radiat Oncol Biol Phys* 1994;29:439–442
50. He Q, Shungu DC, van Zijl PC, Bhujwalla ZM, Glickson JD. **Single-scan in vivo lactate editing with complete lipid and water suppression by selective multiple-quantum-coherence transfer (Sel-MQC) with application to tumors.** *J Magn Reson B* 1995;106:203–211
51. Segebarth CM, Baleriaux DF, Luyten PR, den HJ. **Detection of metabolic heterogeneity of human intracranial tumors in vivo by ^{1}H NMR spectroscopic imaging.** *Magn Reson Med* 1990;13: 62–76
52. Brown TR, Kincaid BM, Ugurbil K. **NMR chemical shift imaging in three dimensions.** *Proc Natl Acad Sci U S A* 1982;79: 3523–3526
53. Maudsley AA, Hilal SK, Simon HE, Wittekoek S. **In vivo MR spectroscopic imaging with P-31: work in progress.** *Radiology* 1984;153:745–750
54. Robinson SP, Howe FA, Rodrigues LM, Stubbs M, Griffiths JR. **Magnetic resonance imaging techniques for monitoring changes in tumor oxygenation and blood flow.** *Semin Radiat Oncol* 1998;8:197–207
55. Al-Hallaq HA, River JN, Zamora M, Oikawa H, Karczmar GS. **Correlation of magnetic resonance and oxygen microelectrode measurements of carbogen-induced changes in tumor oxygenation.** *Int J Radiat Oncol Biol Phys* 1998;41:151–159
56. Aboagye EO, Maxwell RJ, Kelson AB, et al. **Preclinical evaluation of the fluorinated 2-nitroimidazole *N*-(2-hydroxy-3,3,3-trifluoropropyl)-2-(2-nitro-1-imidazolyl) acetamide (SR-4554) as a probe for the measurement of tumor hypoxia.** *Cancer Res* 1997;57:3314–3318
57. Dardzinski BJ, Sotak CH. **Rapid tissue oxygen tension mapping using 19F inversion-recovery echo-planar imaging of perfluoro-15-crown-5-ether.** *Magn Reson Med* 1994;32:88–97